Climate Change Initiative
Living Planet Fellowship

2014

Tero Mielonen

FMI

4000112802/14/I-SBo

European Space Agency
Agence spatiale européenne

STANDARD COVER PAGE FOR ESA STUDY CONTRACT REPORTS

ESA STUDY CONTRACT REPORT		
ESA Contract No: 4000112802/14/I-SBo	SUBJECT: Living Planet Fellowship - ITICA	CONTRACTOR: Finnish Meteorological Institute
ESA CR( )No:	No. of Volumes:....1 This is Volume No:....1	CONTRACTOR'S REFERENCE: EOP-S/14/0008/DFB-dr

ABSTRACT:
In this study we investigated the causes of the positive correlation between aerosol optical depth (AOD) and land surface temperature (LST) over several forested regions using AATSR AOD and LST retrievals from the ESA Aerosol_cci and the GlobTemperature projects, respectively. In addition, we used the aerosol climate model ECHAM-HAMMOZ to estimate the significance of different aerosol processes related to the correlation. We found that over the studied regions, biogenic emission could explain the temperature dependence of AOD but the dependence was stronger in the presence of anthropogenic emissions

The work described in this report was done under ESA Contract. Responsibility for the contents resides in the

Names of authors: Tero Mielonen

NAME OF ESA STUDY MANAGER: Stephen Plummer DIV: EOP-SC DIRECTORATE: EOP	ESA BUDGET HEADING:E-0073-01-L

CCI Living Planet Fellowship Final report

Does Increasing Temperature Increase Carbonaceous Aerosol Direct Radiative Effect over Boreal Forests?

Tero Mielonen
ITICA

Introduction

Aerosol particles are an important regulator of the Earth's climate. They scatter and absorb incoming solar radiation and thus cool the climate by reducing the amount of energy reaching the atmospheric layers and the surface below (direct effect) (e.g., Charlson et al., 1992). A certain subset of the particles can also act as initial formation sites for cloud droplets (cloud condensation nuclei, CCN) and thereby modify the microphysics, dynamics, radiative properties and lifetime of clouds (indirect effects) (Albrecht, 1989; Twomey, 1991; Stevens and Feingold, 2009). The magnitude of aerosol radiative effects remains the single largest uncertainty in current estimates of anthropogenic radiative forcing (International Panel on Climate Change, 2013).

One of the key quantities needed for accurate estimates of the anthropogenic radiative forcing is an accurate estimate of radiative effects from natural aerosol – after all, it is the change from the natural background that is important when quantifying human effects on climate. In fact, recent studies have highlighted that uncertainties in natural aerosol emissions may bias our current estimates of aerosol forcing more than uncertainties associated with anthropogenic emissions (Carslaw et al., 2013). Furthermore, it is highly likely that future changes in regional climate, in terms of, e.g., temperature, precipitation and wind speed, will significantly modify the emissions of natural aerosols and thus severely alter the total aerosol radiative effect in the coming decades. However, our current understanding of future changes in natural aerosol radiative effects is very limited.

The dominant source of natural aerosols over the Earth's vast forested regions are biogenic volatile organic compounds (BVOC) which, following oxidation in the atmosphere, can condense onto aerosol particles to form secondary organic aerosol (SOA) and significantly modify the particles' properties. In accordance with the expected positive temperature dependence of BVOC emissions (Penuelas and Staudt, 2010; Duncan et al., 2009), several previous studies have shown that some aerosol properties, such as mass and ability to act as CCN, also correlate positively with temperature at many forested sites (e.g. Tunved et al., 2006; Leaitch et al., 2011; Paasonen et al., 2013). The evidence for an effect of temperature on aerosol direct effects due to increased BVOC emissions, however, is less clear. Aerosol direct effects can be quantified via aerosol optical depth (AOD) observed from, e.g., satellites. Slowik et al. (2010) explained their observations of enhanced SOA and AOD downwind from a forested area in clear air, unaffected by forest fires or anthropogenic influences, by enhanced biogenic VOC emissions during an episode with high temperatures. During other periods with high temperatures the effects observed at their site, north of Toronto, were much smaller because in addition to temperature, for example, other meteorological effects and biological factors affect the SOA yield. They also discuss that a significant regional radiative cooling effect of the biogenic VOC emissions is to be expected. Similarly, Goldstein et al. (2009) detected an exponential temperature dependence of AOD in the southeastern US, and hypothesized it to arise from enhanced natural BVOC emissions on warmer days. The links between temperature, BVOC emissions and AOD are further complicated over isoprene emitting forests, such as in the southeastern US, by the effect of isoprene oxidation on sulphate aerosol formation: a major oxidation product of isoprene is peroxides, which are generally attributed to the increased summertime formation of sulphate via aqueous phase reactions (Goldstein et al., 2009).

The goal of the ITICA project was (1) to investigate whether a similar temperature effect on AOD can be observed over the remote boreal forest region (about 50° N to 70° N) using remote sensing instruments, with a focus on Eurasia; and (2) if indeed a correlation between AOD and temperature is observed, to also quantify the influence of rising temperatures on the direct radiative effect of aerosols over the boreal forest. This was done to illuminate potential future feedback mechanisms

due to interactions between climate change, biogenic emissions and aerosol radiative effects. Boreal forests were chosen as the study region because they constitute 29 % of the world's forest cover.

In this study, the most important source of observational information over the vast boreal area, where very few in-situ observations are available, is provided by satellites, together with model studies on the underlying chemical and physical processes. The AOD over the boreal forest is typically very low (on the order of 0.1 and smaller; e.g., Aaltonen et al., 2011), except in the presence of biomass burning smoke or pollution transported from industrialized regions. Therefore, the methods applied in the ITICA study were first tested over the same region in the southeastern US which was investigated by Goldstein et al. (2009), aiming at similar effects, but with different methods and instruments, and for a different period of time, to confirm that the selected methods provide results similar to those reported previously. In this research, we planned to analyse the years from 2002 to 2012 (full mission of ENVISAT) but due to the temporal availability of the ancillary satellite products we concentrated on the years 2005 to 2011.

Hypotheses/objectives

The hypotheses tested in this study were:

H1. Higher temperature leads to the increased emission of aerosol precursors

H2. The increased emission of aerosol precursor gases leads to the formation of aerosol particles which grow into the optical active size range and thus increase the AOD such that the AOD increase can be observed from space

H3. The described biosphere–atmosphere interaction leads to a negative feedback in warming climate

H1 was tested by implementing a state-of-the-art biogenic emission scheme into the aerosol-climate model and comparing the model outputs with in-situ measurements of organic aerosol mass around the world. This was done in collaboration with another project which concentrates on model development regarding biogenic emissions.

H2 was tested with satellite observations by analysing AOD retrievals over the southeastern US and boreal forests as a function of temperature. If the temperature dependent biogenic emissions affect AOD it should increase as temperature increases.

H3 was tested using satellite observations and model results by calculating regional and global direct radiative effects and comparing them to see if the modelled and observed aerosol effects are in agreement and how they compare with previously published estimates.

The main objective of this study which addresses all three hypotheses was to investigate the causes of the observed effect of increasing temperatures on the aerosol direct radiative effect, and to provide quantitative estimates of this effect and the resulting negative feedback in a warming climate. More specifically:

O1: The causes of the positive correlation between AOD and LST anomalies that has been observed over the southeastern US were investigated. Possible candidates were: 1) Increasing BVOC emissions with increasing temperature causing SOA formation in the atmospheric boundary layer (**H1**), 2) increasing SOA formation in aqueous phase droplets, and 3) increased biomass burning aerosols with increasing temperature.

O2: Similar AOD-LST correlations were sought for over boreal regions where biogenic emissions are a significant source of atmospheric particles (Spracklen et al., 2008). However, a possible enhanced AOD (**H2**) due to increased emissions of aerosol precursors in response to enhanced temperatures had to be separated from similar effects induced by particles transported from elsewhere.

O3: The significance of the negative feedback caused by a possible warming-induced increase in the aerosol direct radiative effect was estimated with climate model simulations (**H3**).

Methodological approach

In view of the goal of the ITICA study to determine a relation between AOD and temperature changes over remote areas in Eurasia, satellite data are crucial because ground-based information is very sparse. Consequently, many remote sensing data sets were utilized in the project (Table 1). The core data sets for the study were provided by the Advanced Along Track Scanning Radiometer (AATSR) that flew on the ESA polar orbiting Environmental Satellite, ENVISAT (2002-2012):

AATSR AOD data available from the ESA Aerosol_cci project and
AATSR LST data from ESA's GlobTemperature project.
A more detailed description of these products is provided below.

For AOD, the product available from the AATSR Dual View algorithm ADV (Kolmonen et al., 2016) was selected for three reasons:

(1) the three AATSR AOD data sets produced in Aerosol_cci are very similar,
(2) of these three data sets the ADV shows the best agreement with the AOD retrieved from the Multi-angle Imaging SpectroRadiometer (MISR) which has been used in a similar analysis (Goldstein et al., 2009),
(3) the providers are part of the ITICA team, thus first-hand knowledge on data characteristics is available.

Over land, the AATSR dual-view algorithm ADV (Kolmonen et al., 2016) uses both nadir and forward view measurements of top-of-the-atmosphere (TOA) reflectances at three wavelengths (0.555, 0.659, and 1.61 μm) to decouple atmospheric and surface contributions to the observed signal. The algorithm retrieves the mixture of four aerosol components (non-absorbing fine, absorbing fine, sea salt, and dust) which best describes the observed TOA reflectances. This mixture defines the columnar aerosols properties and the corresponding AOD at each of three wavelengths. The algorithm's main assumption is that the ratio of the surface reflectance measured in the forward and the nadir views is independent of the wavelength. The main product of the retrieval is AOD, including pixel level uncertainties. For a more detailed description of the algorithm see (Kolmonen et al., 2016) and the algorithm's ATBD (http://www.esa-aerosol-cci.org/?q=products%20description).

The AOD data used were Daily Level 3 with spatial resolution of 1° × 1° from the full mission (2002-2012). The Level 3 AOD product is an average of the Level 2 AOD product (10 × 10 km^2) which is retrieved from cloud-cleared observations. After the retrieval, the Level 2 AOD values are post-processed to remove the remaining cloud contamination. The Level 3 data with spatial resolution of 1° × 1° was chosen because it is close to the spatial resolution of climate models. Although the inclusion of ATSR-2 would have provided data starting from 1995, no ancillary data on atmospheric constituents (e.g. CO, NO_2), which are needed for identification of the occurrence of different aerosol species, are available for that time period.

The LST algorithm uses pixel-by-pixel TOA radiometrically and geometrically calibrated brightness temperatures from the nadir split-window (11 and 12 μm) channels of the AATSR. The retrieval coefficients are dependent on the biome, fractional vegetation cover, precipitable water, satellite zenith view angle, and the time of day (day or night). Ancillary information is used to correct for water vapour absorption and spectral emissivity effects. Regarding aerosol correction, the LST algorithm uses dust optical depth from the SU CCI product to mask pixels where aerosol may be effecting the observed LST (AOD > 0.2) to capture dust events in China and Africa. In the regions analyzed in this study, the aerosol loads/sizes are not high enough to affect the LST retrieval. The LST product is generated using a regression relation and look-up tables that accommodate global and seasonal variations in the main perturbing influences. Both the fractional vegetation cover and precipitable water are seasonally dependent whereas the biome is invariant. The Level 3 product exploited here

has been cloud-cleared and re-gridded onto a regular equal-angle grid. For more information, see the AATSR LST Algorithm Theoretical Basis Document (Prata, 2002) and the Validation Report (Ghent, 2012).

Table 1. Satellite products used in the project.

Instrument (data depository)	Product	Product type	Usage
AATSR (Aerosol_cci/ESA)	Aerosol optical depth	Level 3, 1° × 1°, daily	Amount of aerosols
AATSR (GlobTemperature/ESA)	Land surface temperature	Level 3, 0.01° × 0.01°, daily	Temperature
AIRS (ACDISC/NASA)	Carbon monoxide column	Level 3, 1° × 1°, daily	Proxy for biomass burning aerosols
AIRS (ACDISC/NASA)	Atmospheric water vapour	Level 3, 1° × 1°, daily	Water content of the atmosphere
GOME	Sun-induced fluorescence	Level 3, 1° × 1°, monthly	Proxy for plant photosynthesis
MISR	Aerosol optical depth	Level 3, 1° × 1°, monthly	Amount of aerosols
MODIS	Cloud optical depth, Cloud fraction	Level 3, 1° × 1°, monthly	
MODIS	Land cover type	Level 3, 0.05° × 0.05°, annual	Proxy for vegetation type
MODIS	Thermal anomalies	Daily, gridded to 1° × 1°	Fire locations
OMI	Formaldehyde	Level 3, 1° × 1°, daily	Proxy for SOA load
OMI (ACDISC/NASA)	Tropospheric nitrogen dioxide	Level 3, 0.25° × 0.25°, daily	Proxy for pollution aerosols
OMI (ACDISC/NASA)	Columnar sulphur dioxide	Level 3, 0.25° × 0.25°, daily	Proxy for pollution aerosols
OMI (ACDISC/NASA)	Surface UV radiation	Level 3, 1° × 1°, daily	Proxy for incoming radiation
CALIOP (ASDC/NASA)	Aerosol profile	Level 3, 2° × 5° deg, monthly	Vertical location of aerosols
SCIAMACHY	Sun-induced fluorescence	Level 3, 1° × 1°, monthly	Proxy for plant photosynthesis
SMMR, SSM/I, TMI, AMI-WS, ASCAT, AMSR-E, WindSat, AMSR2 (Soil Moisture_cci/ESA)	Soil moisture	Level 3, 0.25° × 0.25°, daily	Proxy for plant condition

AOD retrieved from satellite radiance data contains contributions from all aerosol types present in the atmospheric column. To discriminate natural contributions to the AOD from other contributions (such as aerosol particles emitted by forest fires or pollution transported from elsewhere), ancillary data were used. Daily Level 3 carbon monoxide (CO) column concentration data retrieved from NASA's Atmospheric Infrared Sounder (AIRS) for the years 2002-2012 were used as a proxy for biomass burning aerosols (smoke). In addition, Level 3 total column water vapour measurements from the same instrument were used in the evaluation of model output and in the analysis of the satellite based AOD-LST relationship. Other NASA products used in the analysis were tropospheric NO_2, columnar SO_2, formaldehyde, and surface UV from the Ozone Monitoring Instrument (OMI), AOD from MISR, cloud properties, land cover type and thermal anomalies from the Moderate Resolution Imaging Spectroradiometer (MODIS), sun-induced fluorescence from the Global Ozone Monitoring Experiment (GOME) and the Scanning Imaging Absorption SpectroMeter for Atmospheric CHartographY (SCIAMACHY) and aerosol profiles from the Cloud-Aerosol Lidar with Orthogonal Polarization (CALIOP).

NO_2 and SO_2 were used to identify aerosols that are mixed with anthropogenic pollution (Veefkind et al., 2011). OMI formaldehyde data were used to estimate the amount of SOA and OMI UV data were used to estimate the amount of radiation reaching the surface. Daily Level 3 OMI data are available from 2005 onwards. Sun-induced fluorescence data available from GOME and SCIAMACHY were used to estimate the amount of plant photosynthesis. MODIS Land cover type data were used to identify the main vegetation types in each pixel and the MODIS cloud product to estimate the relationship between aerosols and clouds. Daily Level 3 MODIS data are available from 2000 onwards. The Level 3 aerosol profiles from CALIOP are monthly data with 2 × 5 degrees spatial resolution, which are available from 2006 onward. The CALIOP profiles were used to evaluate the vertical distribution of aerosols in the studied regions. Finally the Soil Moisture_cci homogenized and merged soil moisture product, which provides daily surface soil moisture with a global coverage and a spatial resolution of 0.25, were used in the evaluation of model output and in the analysis of the satellite-based AOD-LST relationship. Because the reliability of the SM_cci product depends on the forest density, regions with the highest uncertainties (e.g. dense forests) were not included in the analysis.

Most of the above-mentioned products did not present clear relationships with the studied parameters (AOD, LST), thus in the results section we only discuss the NO_2 and CO observations. A more detailed discussion on the other satellite products can be found in the project's previous reports.

In order to estimate the effect of SOA on the AOD-LST relationship, we applied the ECHAM6-HAMMOZ aerosol-chemistry climate model (Stier et al., 2005; Zhang et al., 2012; Bergman, et al. 2012; Laakso et al. 2016). Biogenic VOC emissions are computed online using the Model of Emissions of Gases and Aerosols from Nature (MEGAN, Guenther et al., 2006). MEGAN determines emissions of terpenes and isoprenes as a function of temperature, available solar radiation, soil moisture, and carbon dioxide concentration (for which a fixed global average is used). In order to couple MEGAN emissions with atmospheric SOA formation in the model, a scheme based on the volatility basis set (VBS) (Donahue et al., 2011) was introduced. It enabled the modelling of the condensation and evaporation of semi-volatile organic compounds (sVOC). These schemes enabled the simulation of the effects of temperature changes on atmospheric aerosol load. For biomass burning, the Global Fire Emissions Database (GFEDv2) was used. Newer versions of the emission database (GFED4 and GFED4s) have been published but they are not yet available in a suitable input format for ECHAM6-HAMMOZ.

In addition to SOA formation in the boundary layer, Ford and Heald (2013) speculated that another cause for AOD-LST correlation over the southeastern US could be SOA formed in the aerosol liquid phase. To estimate this contribution, a parameterization that describes aqueous SOA formation was implemented in the model.

The new schemes were based on the best available methods for the numerical description of the processes involved. However, no estimates on the uncertainty of these schemes were available, thus error propagation through the models could not be done. Typically, the quality of the schemes implemented into climate models is evaluated by comparing the old and the new model version with observations. Such a comparison was done in collaboration with another project and these results are included in the results section.

The model can be used for free-running simulations or the model meteorology can be nudged towards reanalysis data. In this study, the years 2002-2010 were simulated because for these years we have the emission inputs and satellite observations required for the comparison. Simulations are nudged using the ECMWF reanalysis data to ensure compatibility between the model and the observed atmospheric conditions.

To study how different aerosol sources affect the aerosol load over the studied regions, four model runs were made: 1) CONTROL: all the schemes described above are in use, 2002-2010, daily averages, 2) noBB: same as CONTROL but without biomass burning emissions, 3-hourly averages, 3) noAQSOA: same as CONTROL but without SOA formed in aqueous phase, 3-hourly averages, 4) noBIOSOA: same as CONTROL but without biogenic SOA formation, 3-hourly averages. The importance of each aerosol

source was estimated by comparing the model run without that source to the CONTROL run.

To study the aerosol feedback effect in the future, two simulations from 2045 to 2055 using the RCP8.5 scenario for the year 2050 were made: 1) FUTURE_CONTROL: all the schemes described above are in use, monthly averages, 2) FUTURE_noBIOSOA: same as CONTROL but without biogenic SOA formation, monthly averages. The RCP8.5 scenario was chosen because it represents the highest temperature increase in the scenarios and thus it provides the best opportunity to detect and quantify a globally significant negative aerosol feedback.

The objectives of this project were addressed in three work packages (WPs), one for each specific objective (**O1-O3**). The overall study approach is illustrated in Figure 1, which shows the work flow between the analysis of satellite data and modelling.

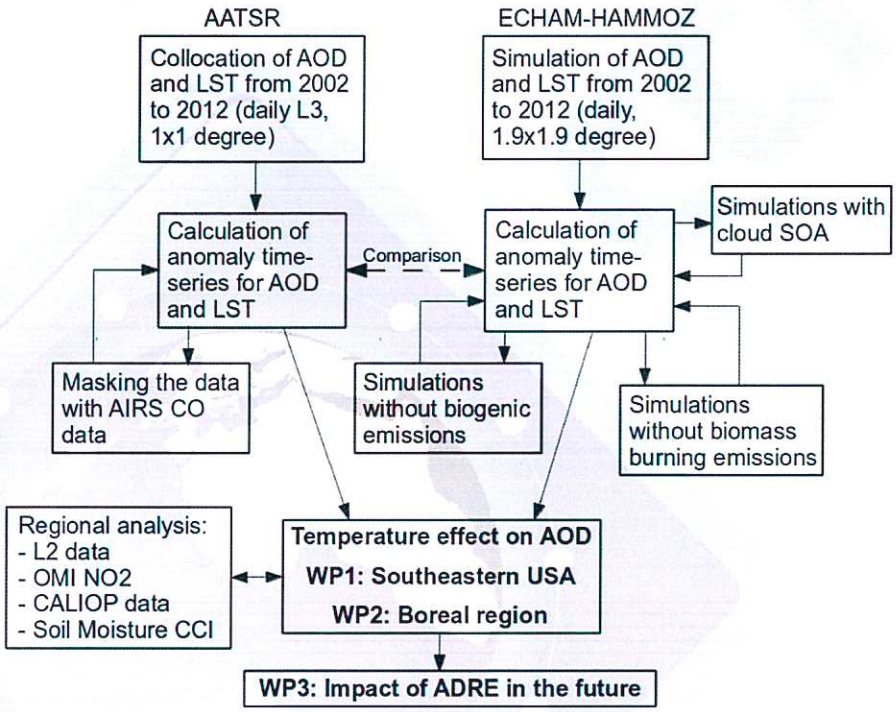

Figure 1. Schematic representation of the methodology applied to study the temperature effect on AOD (WP1 and WP2) and consequences on the possible feedback between biosphere and atmosphere (WP3). AOD refers to aerosol optical depth, LST to land surface temperature, SOA to secondary organic aerosols, and ADRE to aerosol direct radiative effect.

Results

To ascertain that the model could be used to test Hypothesis 1 (H1) we evaluated the biogenic aerosol masses in the CONTROL simulation using observations done with the Aerodyne Aerosol Mass Spectrometer (AMS) around the globe. The AMS datasets were downloaded from the Aerosol Mass Spectrometry (AMS) Global Database where they are freely available (Zhang et al., 2017). In the comparisons, monthly averages of the months corresponding to the respective measurement periods were used, although it is worth noting that the measurement campaigns were shorter than a month. The comparisons were made for three different surroundings (urban, urban downwind and rural & remote).

Overall, the simulated organic masses are in the same size range but slightly smaller than the measured ones. Regarding the performance of the model in the southeastern US and the boreal regions, AMS measurements were available from only 3 sites in the US (shown in Figure 2): two East

Coast Cruises (de Gouw et al., 2005) and Duke Forest (Stroud et al., 2007). There, the model and the in-situ observations are in excellent agreement which gives confidence that the model is suitable for studying biogenic aerosols in this region. This analysis was done in collaboration between the ITICA project and a model development project. A more detailed evaluation of these results will be published in a peer-reviewed article which describes the developed model version.

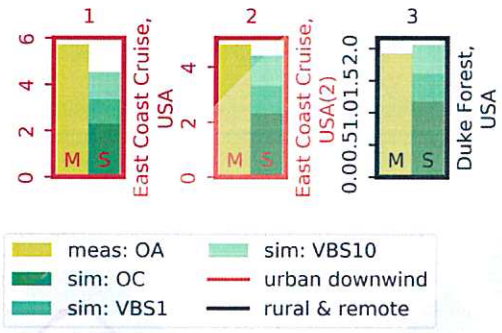

Figure 2. Measured (meas) and simulated (sim) organic aerosol (OA) mass concentrations (μg/m³) in the southeastern US. The comparison is based on monthly averages. OC, VBS1 and VBS10 refer to non-volatile, low-volatile and semi-volatile VOCs.

Work package 1

In the first work package (WP1) we estimated the AOD-LST dependency over the southeastern US (70-90°W, 30-37.5°N) and approximated the radiative effects of this dependence. The studied region and the most common vegetation types there are shown in Figure 3. We calculated the anomalies of LST and AOD for the individual 1° × 1° pixels for the summers (averages over the months June, July, and August). Seasonal averages were calculated from monthly averages to ensure that each month had an equal weight in the seasonal average. The anomalies were calculated by subtracting the average of all the summers from the yearly summer averages.

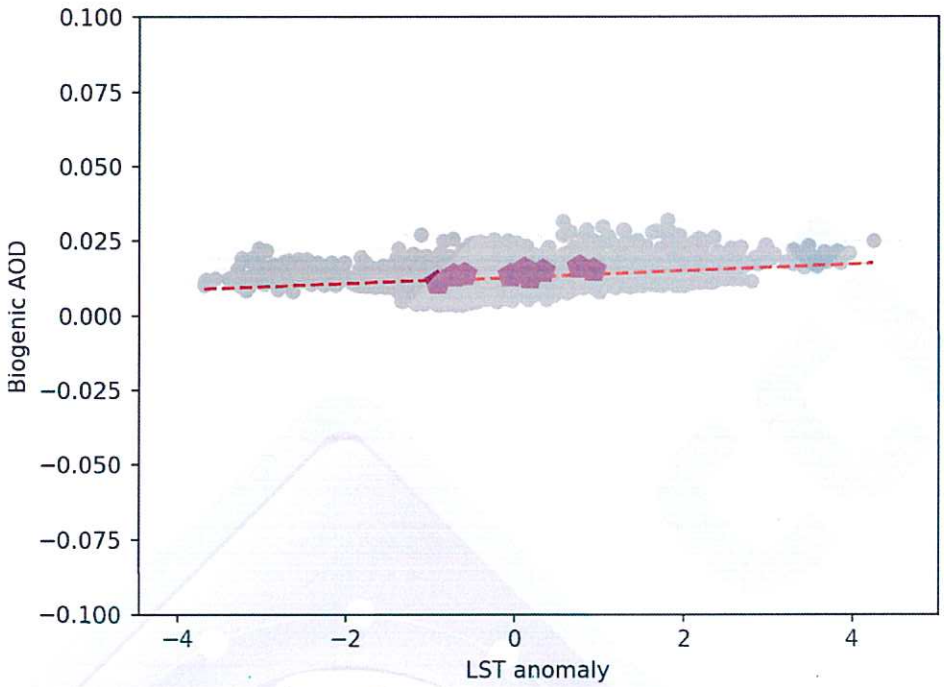

Figure 12. Biogenic AOD (based on the difference between the CONTROL and the noBIOSOA simulations) vs. LST anomaly for the summers (JJA) of 2002-2010 over Canada. Pentagons represent the averages over the whole domain (80-130°W, 50-63°N) while the dots represent 1.9° × 1.9° pixels within the domain. The dashed line represents the linear fit to the individual pixels ($AOD_{bio} = 0.0011 LST_{ano} + 0.001$), the red curtain represents the 90 % credible interval for the linear fit and the error bars represent the uncertainty caused by averaging.

Eastern Russia

Over the mixed forests in eastern Russia (11 pixels) there is a positive temperature dependence in summertime AOD as shown in Figure 13. AOD increases by (25±10) × 10^{-4} K^{-1}. The columnar CO concentrations also exhibit a positive dependence on temperature (177±13) × 10^{14} K^{-1} but the dependence between AOD and CO appears to be negative: (-27±4) × 10^{-19} $(molecules/cm^2)^{-1}$. There is no clear relation between AOD and tropospheric NO_2 concentrations, thus anthropogenic emissions do not have a clear effect on the AOD levels in this region. As the CO and tropospheric NO_2 observations do not indicate that the temperature dependence of AOD is caused by either biomass burning or anthropogenic emissions, no correction is needed. Thus, we compared the observed dependency of the total AOD with the simulations of biogenic emissions. The simulated temperature dependence of the biogenic AOD for this region is shown in Figure 14. The simulated temperature dependence for biogenic AOD is smaller ((12±2) × 10^{-4} K^{-1}) but still in the same range as the observational estimate for the total AOD.

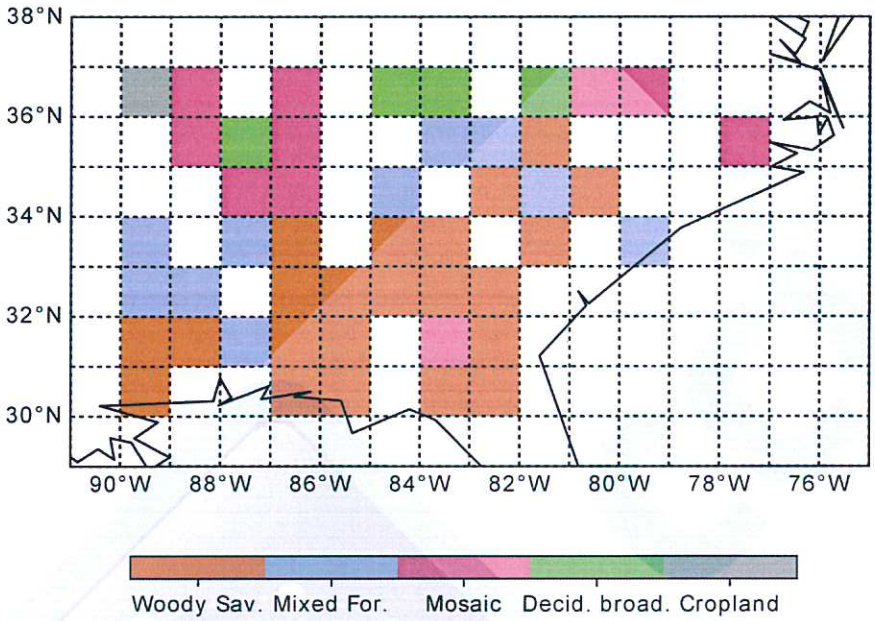

Figure 3. The most common vegetation types in the southeastern US based on the MODIS MCD12C1 product for the year 2011. Land cover types are classified according to IGBP. A 1° × 1° pixel was considered to be dominated by a certain land cover class if the fraction of that type was 0.5 or larger in the pixel. The five most common land cover classes in 2011 were: woody savannas (22 pixels), mixed forests (13 pixels), cropland/natural mosaic (10 pixels), deciduous broadleaf forests (4 pixels) and cropland (1 pixel).

When the summertime tropospheric NO_2 column densities from the summers 2005-2011 are compared to the corresponding AOD values, a linear dependence can be seen, as the linear fit with 90 % credible intervals in Figure 4 shows. As the tropospheric NO_2 is predominantly from anthropogenic sources (Veefkind et al., 2011), the figure indicates that the summertime AOD levels in this region are closely related to the amount of anthropogenic emissions.

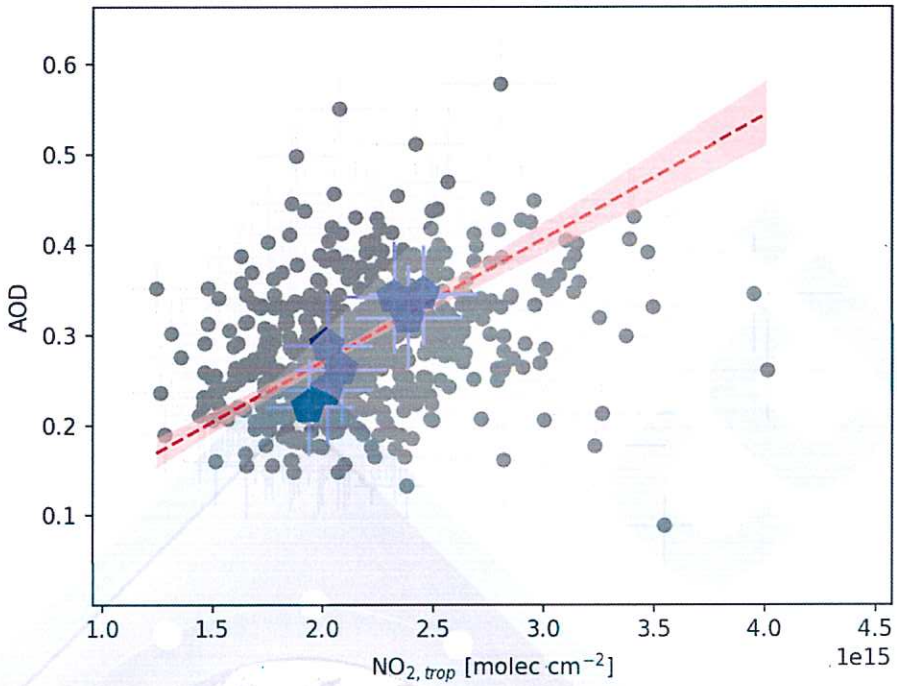

Figure 4. Summertime (JJA) averages of AOD vs. tropospheric NO_2 over the southeastern US for the years 2005–2011. Pentagons represent the averages over the whole domain (70-90°W, 30-37.5°N) while the dots represent 1° × 1° degree pixels within the domain. AOD is from L3 AATSR and tropospheric NO_2 from L3 OMI. The error bars represent the uncertainty of the observations. The linear fit shown with the red dashed line is based on the 1° × 1° degree pixels ($\mathrm{AOD} = 1.31e^{-16}\mathrm{NO}_{2,\mathrm{trop}} + 0.013$). The red curtain represents the 90 % credible interval for the linear fit.

The competition between the effects of anthropogenic emissions and the temperature-dependent BVOC emissions on the AOD was investigated for the first time by separating the AATSR AOD anomalies into anthropogenic and non-anthropogenic components using tropospheric NO_2 observations from OMI. In practice, we first extracted an estimated anthropogenic AOD contribution from the total AOD. The anthropogenic contribution was calculated using the linear fit between the summertime AOD and tropospheric NO_2 columns ($\mathrm{AOD} = 1.31e^{-16}\mathrm{NO}_{2,\mathrm{trop}} + 0.013$, Figure 4). In addition to the uncertainties of the observed AOD and tropospheric NO_2 concentrations, the uncertainty of the linear fit was also taken into account. The non-anthropogenic AOD was then estimated by subtracting the anthropogenic AOD from the total AOD. Then we calculated the summertime anomalies for the anthropogenic and non-anthropogenic AODs for each of the 1° × 1° pixels within the studied domain. This analysis showed that anthropogenic AOD is not temperature dependent but the non-anthropogenic AOD has a small dependence on temperature ((60±40) × 10^{-4} K^{-1}) as shown in Figure 5. Our model simulations (summers 2002-2010) produced comparable temperature dependence in the biogenic AOD over the southeastern US as shown in Figure 6. The model showed that the increase in AOD due to BVOC emissions was (35±5) × 10^{-4} K^{-1}, which is within the uncertainty range of the observed change in the non-anthropogenic AOD.

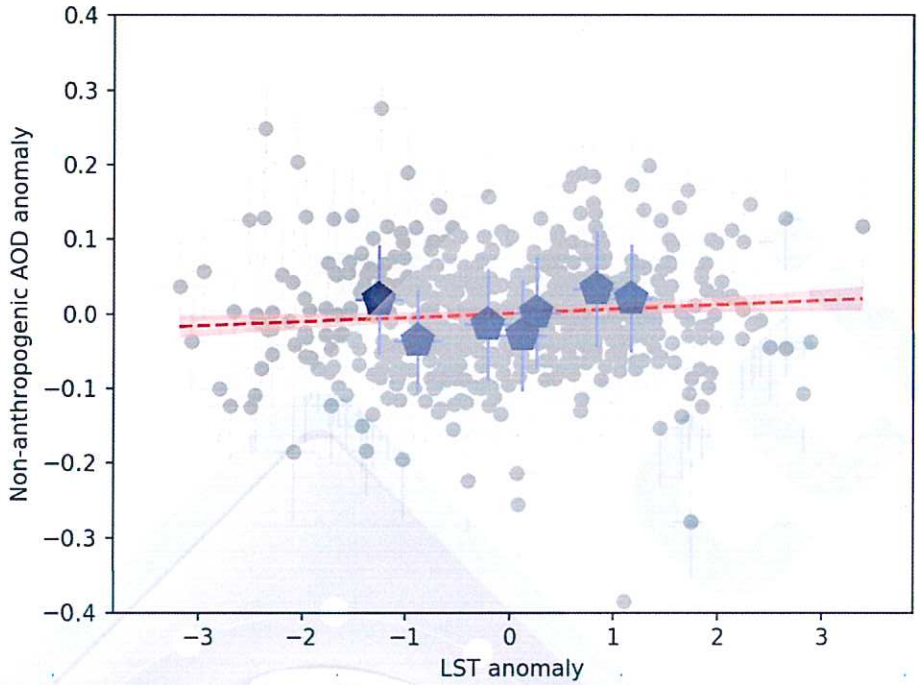

Figure 5. Summertime (JJA) anomalies of non-anthropogenic AOD vs. LST, for the years 2005–2011 over the southeastern US. The non-anthropogenic AOD has been determined based on L3 AATSR AOD and OMI tropospheric NO_2 observations as described in the text. LST is from L3 AATSR. Pentagons represent the averages over the whole domain (70-90°W, 30-37.5°N) while the dots represent 1° × 1° pixels within the domain. The dashed line represents the linear fit to the 1° × 1° degree pixels ($\mathrm{AOD_{NA,ano}} = 0.006\mathrm{LST_{ano}} - 0.001$), the red curtain represents the 90 % credible interval for the linear fit and the error bars represent the uncertainty of the data points.

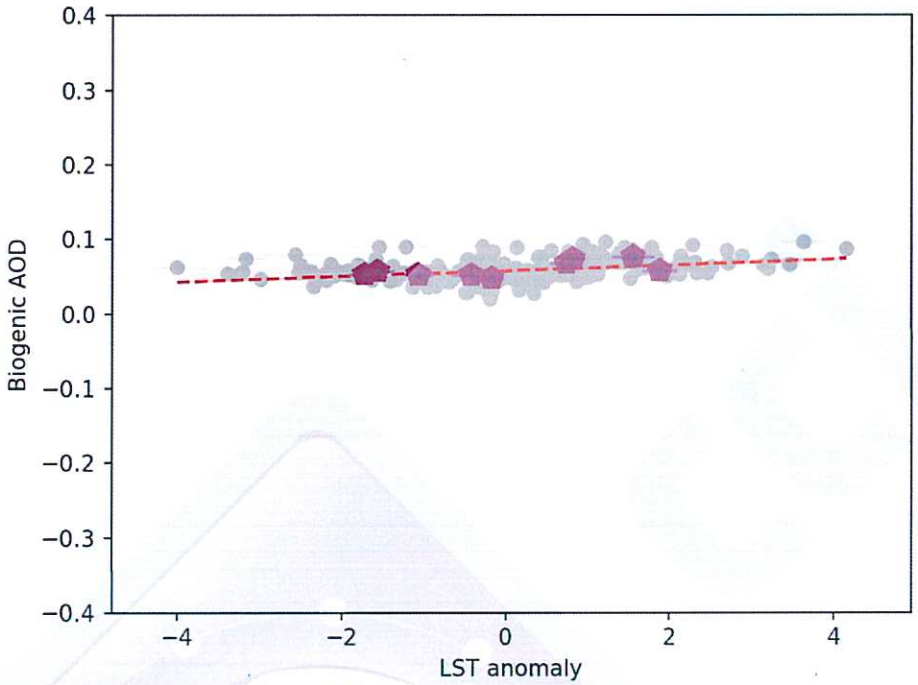

Figure 6. Biogenic AOD (based on the difference between the CONTROL and the noBIOSOA simulations) vs. LST anomaly for the summers (JJA) 2002-2010 over the southeastern US. Pentagons represent the averages over the whole domain (70-90°W, 30-37.5°N) while the dots represent 1.9° × 1.9° pixels within the domain. The dashed line represents the linear fit to the individual pixels ($AOD_{bio} = 0.0035LST_{ano} + 0.056$), the red curtain represents the 90 % credible interval for the linear fit and the error bars represent the uncertainty caused by temporal averaging.

The largest source of isoprene emissions in the southeastern US are broadleaf trees (Millet et al., 2008; Guenther et al., 2006), thus if the observed temperature dependence of AOD is caused by biogenic emissions the dependence should be larger in the vicinity of forests than in locations with fewer trees. To study this we used the MODIS land cover type classification data and limited the observed data sets to the three most common land cover types: woody savannas (22 pixels out of 82), mixed forests (13 pixels out of 82) and cropland/natural mosaic (10 pixels out of 82) (see Figure 3). Then we did the same analysis as we did for the whole domain for each of the land cover types separately (shown in Figures 7-9) and found that only pixels with mixed forests exhibited a clear temperature dependence for non-anthropogenic AOD.

For the pixels covered mainly by mixed forests (Figure 7) the biogenic contribution increases non-anthropogenic AOD by approximately (260±170) × 10^{-4} K^{-1} which is more than four times larger than for the whole domain. Over the pixels classified as woody savannas the summer 2005 was anomalously cold and due to this exceptional summer there does not seem to be temperature dependence in the biogenic AOD (see Figure 9). However, if the summer of 2005 is discarded from the analysis, the temperature dependence of biogenic AOD over these pixels is in the same range as over mixed forests ((240±140) × 10^{-4} K^{-1}). The increased temperature dependence of the non-anthropogenic AOD in the vicinity of forests supports our assumption that the non-anthropogenic AOD derived from the observations is most likely SOA formed from biogenic VOC emissions. Due to the coarser spatial resolution of the model, the simulation results could not be separated for the different vegetation types.

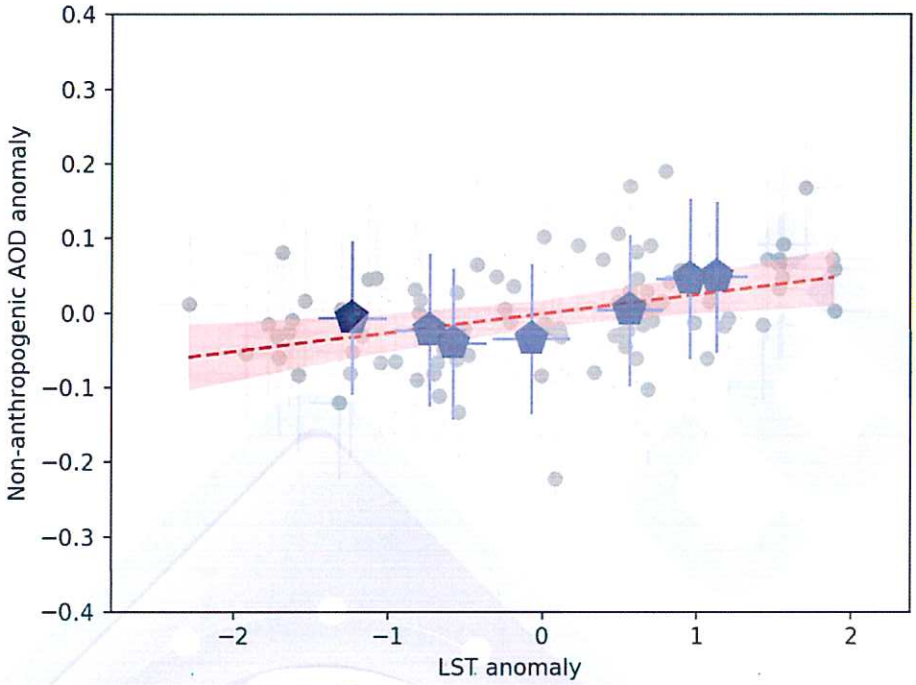

Figure 7. Summertime (JJA) anomalies of non-anthropogenic AOD vs. LST, for the years 2005–2011 over mixed forests in the southeastern US. The non-anthropogenic AOD has been determined based on L3 AATSR AOD and OMI tropospheric NO_2 observations as described in the text. LST is from L3 AATSR. Pentagons represent the averages over the mixed forest pixels (70-90°W, 30-37.5°N) while the dots represent 1° × 1° pixels within the domain. The dashed line represents the linear fit to the 1° × 1° degree pixels ($\mathrm{AOD}_{\mathrm{NA,ano}} = 0.026\mathrm{LST}_{\mathrm{ano}} - 0.0003$), the red curtain represents the 90 % credible interval for the linear fit and the error bars represent the uncertainty of the data points.

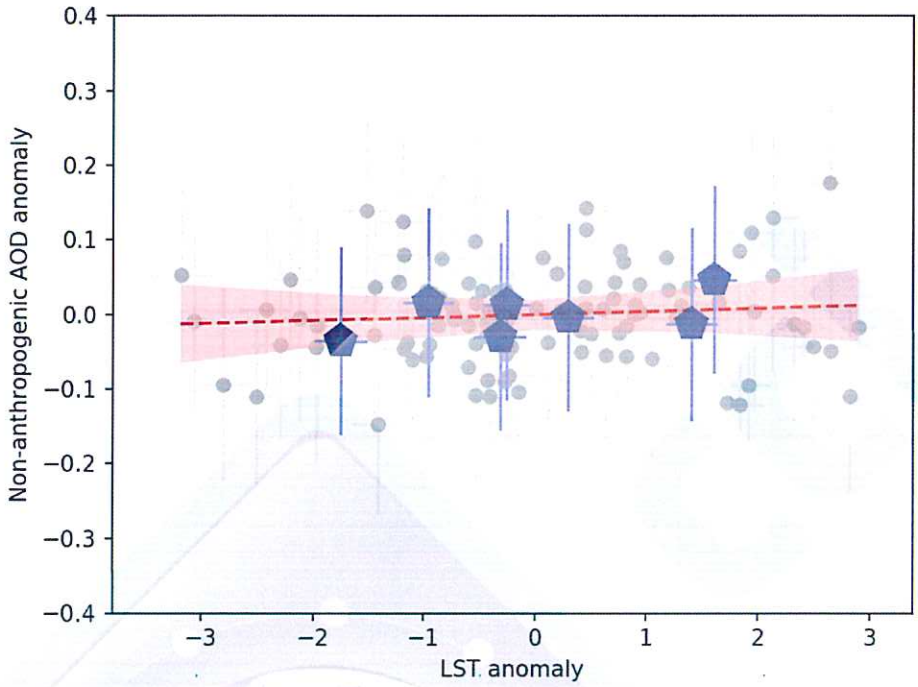

Figure 8. Summertime (JJA) anomalies of non-anthropogenic AOD vs. LST, for the years 2005–2011 over cropland/natural mosaic in the southeastern US. The non-anthropogenic AOD has been determined based on L3 AATSR AOD and OMI tropospheric NO_2 observations as described in the text. LST is from L3 AATSR. Pentagons represent the averages over the cropland/natural mosaic pixels (70-90°W, 30-37.5°N) while the dots represent 1° × 1° pixels within the domain. The dashed line represents the linear fit to the 1° × 1° degree pixels ($\mathrm{AOD_{NA,ano}} = 0.004\mathrm{LST_{ano}} - 0.0001$), the red curtain represents the 90 % credible interval for the linear fit and the error bars represent the uncertainty of the data points.

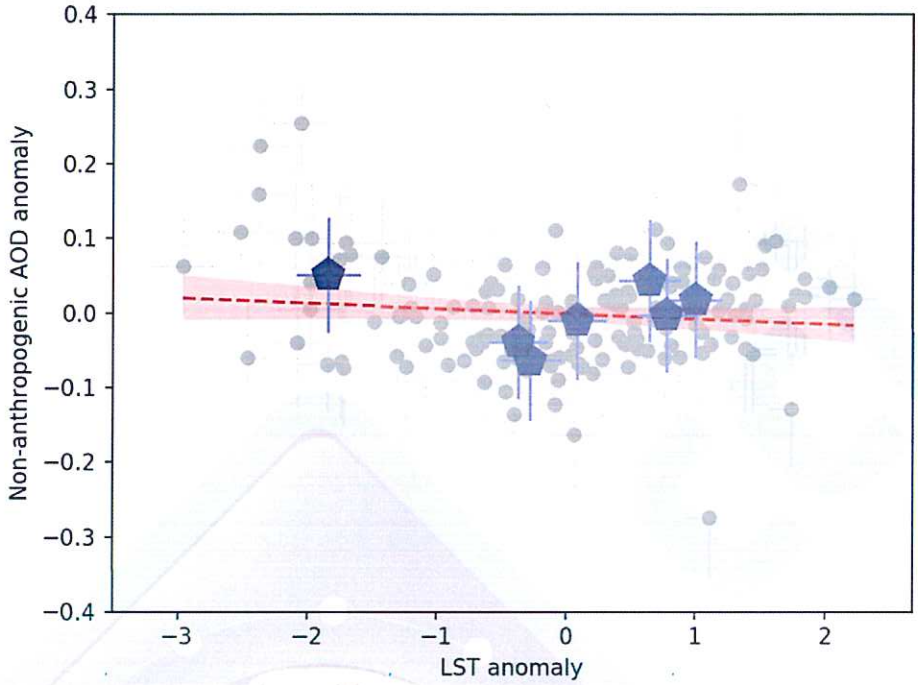

Figure 9. Summertime (JJA) anomalies of non-anthropogenic AOD vs. LST, for the years 2005–2011 over woody savannas in the southeastern US. The non-anthropogenic AOD has been determined based on L3 AATSR AOD and OMI tropospheric NO_2 observations as described in the text. LST is from L3 AATSR. Pentagons represent the averages over the woody savanna pixels (70-90°W, 30-37.5°N) while the dots represent 1° × 1° pixels within the domain. The dashed line represents the linear fit to the 1° × 1° degree pixels ($AOD_{NA,ano} = -0.007LST_{ano} - 0.0005$), the red curtain represents the 90 % credible interval for the linear fit and the error bars represent the uncertainty of the data points.

Using the above-mentioned changes in AOD per temperature degree in the following equation we estimated the regional clear-sky direct radiative effect (DRE) of the non-anthropogenic AOD (e.g. Haywood and Shine, 1995):

$$DRE = S_{rad}\phi\Delta AOD(1-C_c)T_{atm}^2(1-R_s)^2\left(2R_s\frac{1-\varpi}{(1-R_s)^2}-\beta\varpi\right) \quad (1)$$

where S_{rad} is the incident solar radiation (461 W/m^2) at the top of the atmosphere, ϕ is the mean daytime value of the secant of the solar zenith angle (1.33), C_c is the fractional cloud amount (0.0 for clear-sky), T_{atm} is the aerosol free atmospheric transmission (0.76), R_s is the shortwave surface reflectance (0.15), ω is the single scattering albedo (0.972), and β is the up-scatter fraction (0.21). All values for the variables in this equation, except for S_{rad} and ϕ, were taken from Goldstein et al. (2009). The region and season averaged S_{rad} and ϕ were calculated with the help of the tools in the LibRadtran package (Emde et al., 2016). The original equation by Haywood and Shine (1995) was designed for global DRE estimates and it includes global variables day length and solar constant, thus the equation was modified for regional calculations by replacing them with S_{rad} and ϕ to get a regional DRE estimate.

Using these assumptions, the clear-sky DRE of the observation based biogenic AOD is -0.31±0.22 W/m^2/K for the whole domain and -1.28±0.86 W/m^2/K over mixed forests only. The model estimate of the regional clear-sky DRE for biogenic aerosols is similar to that estimated from the observations: -0.34±0.02 W/m^2/K. The observational estimates have larger uncertainties than the simulated ones because we did our best to take into account the uncertainties of the actual observations and the fitting. For the simulations we were only able to consider the uncertainty from the averaging and the fitting. Thus, the model uncertainties are likely underestimated since we were not able to take into

account all sources of uncertainty such as uncertainties in the model parameterizations.

All these DRE values are significantly larger than the values reported for other forested regions (Lihavainen et al., 2015; Paasonen et al., 2013). Furthermore, the model simulations show that biogenic emissions have a significant effect on the indirect radiative forcing in this region. The approximated effective radiative forcing (ERF) for the biogenic aerosols was -1.04±0.22 W/m^2/K which is larger than the values reported for other forested regions (Paasonen et al., 2013).

A manuscript describing these results is in preparation.

Work package 2

In the second work package (WP2), we analysed three boreal regions: one over Canada (80-130°W, 50-63°N) and two over Russia (40-65°E, 59-66°N and 78-100°E, 57-63°N). These regions are shown in Figure 10. They were selected as they are mainly covered by forests, they do not include any large cities and they include at least 10 pixels with observations from all summers between 2005 and 2011. The Canadian region was dominated by evergreen needleleaf forests while the easternmost region in Russia was dominated by mixed forests. The western region in Russia contained both mixed and evergreen needleleaf forests.

To minimize the contribution of biomass burning aerosols (smoke) in the observed AOD values, we used the MODIS Fire radiative power (FRP) and ECMWF ERA-Interim wind direction data in the sampling of the satellite observations following the guidelines presented by Slowik et al. (2010). Only pixels in which the wind was coming from the north (v component smaller than -2 m/s) and which had no FRP value were selected for the analysis. Furthermore, we required that no FRP values were detected in the pixels east and west of the pixel under evaluation and in the next two pixels north of these pixels. This was done to ensure that there were no large fires in the vicinity of the pixel to complicate the analysis with smoke.

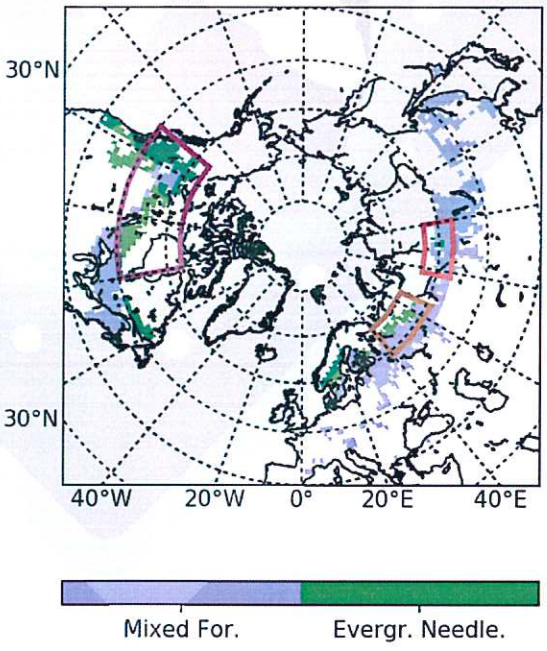

Figure 10. The distribution of mixed and evergreen needleleaf forests in the boreal region. The forest locations and types are based on the MODIS MCD12C1 product for the year 2011. Land cover types are classified according

to IGBP. A 1° × 1° pixel was considered to be dominated by a certain land cover class if the fraction of that type was 0.5 or larger in the pixel. The boxes refer to the regions analysed: evergreen needleaf forests in Canada (purple), evergreen needleaf and mixed forests in western Russia (brown) and mixed forests in eastern Russia (red).

Canada

After the initial data screening we had 13 pixels over evergreen needleleaf forests in Canada. However, three of these pixels were associated with high AOD values (>0.3) and CO concentrations (>2.3 molec/cm^2) during 2008 and 2010. The Canadian National Fire Database (http://cwfis.cfs.nrcan.gc.ca/ha/nfdb) revealed that these pixels were in the vicinity of large forest fires during these years. Therefore, as the high AOD values were associated with high CO concentrations in the vicinity of fires, the summer averages were most likely affected by smoke, and we discarded these pixels from the analysis. The remaining 10 pixels exhibit a very small and highly uncertain temperature dependence in AOD: (8±30) × 10^{-4} K^{-1} (shown in Figure 11).

The simulated temperature dependence of the biogenic AOD for this region is shown in Figure 12. It is slightly larger ((11±1) × 10^{-4} K^{-1}) but still in the same range as that estimated from the observations. These results indicate that the biogenic emissions over the evergreen needleleaf forests in Canada likely have a small temperature dependent effect on the AOD which however is barely detectable with remote sensing observations.

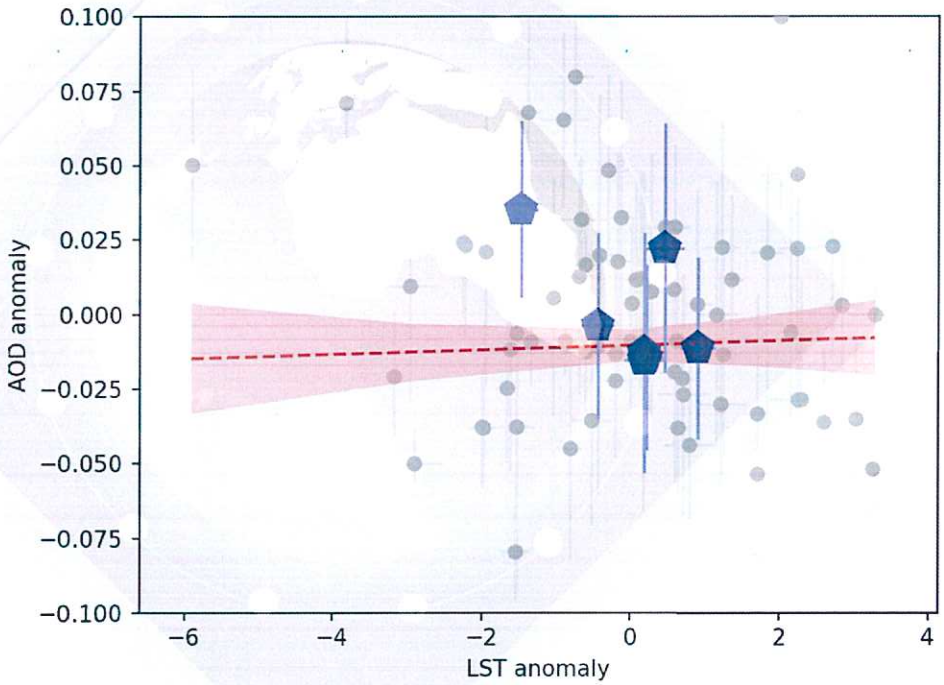

Figure 11. Summertime (JJA) anomalies of AOD vs. LST, for the years 2005–2011 over evergreen needleleaf forests in Canada. The non-smoke AOD has been determined based on L3 AATSR AOD and AIRS columnar CO observations as described in the text. LST is from L3 AATSR. Pentagons represent the averages over the evergreen needleleaf pixels (80-130°W, 50-63°N) while the dots represent 1° × 1° pixels within the domain. The dashed line represents the linear fit to the 1° × 1° degree pixels ($AOD_{NS,ano} = 0.0008LST_{ano} - 0.01$), the red curtain represents the 90 % credible interval for the linear fit and the error bars represent the uncertainty of the data points.

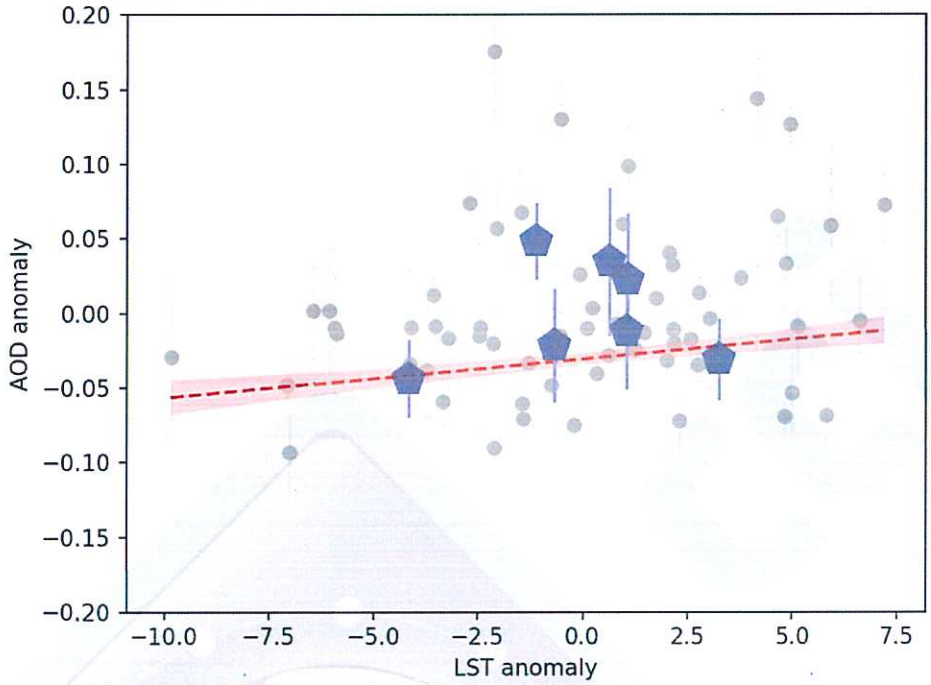

Figure 13. Summertime (JJA) anomalies of total AOD vs. LST, for the years 2005–2011 over mixed forests in eastern Russia. The AOD and LST are from L3 AATSR. Pentagons represent the averages over the mixed forest pixels (78-100°E, 57-63°N) while the dots represent 1° × 1° pixels within the domain. The dashed line represents the linear fit to the 1° × 1° pixels ($AOD = 0.0025LST_{ano} - 0.003$), the red curtain represents the 90 % credible interval for the linear fit and the error bars represent the uncertainty of the data points.

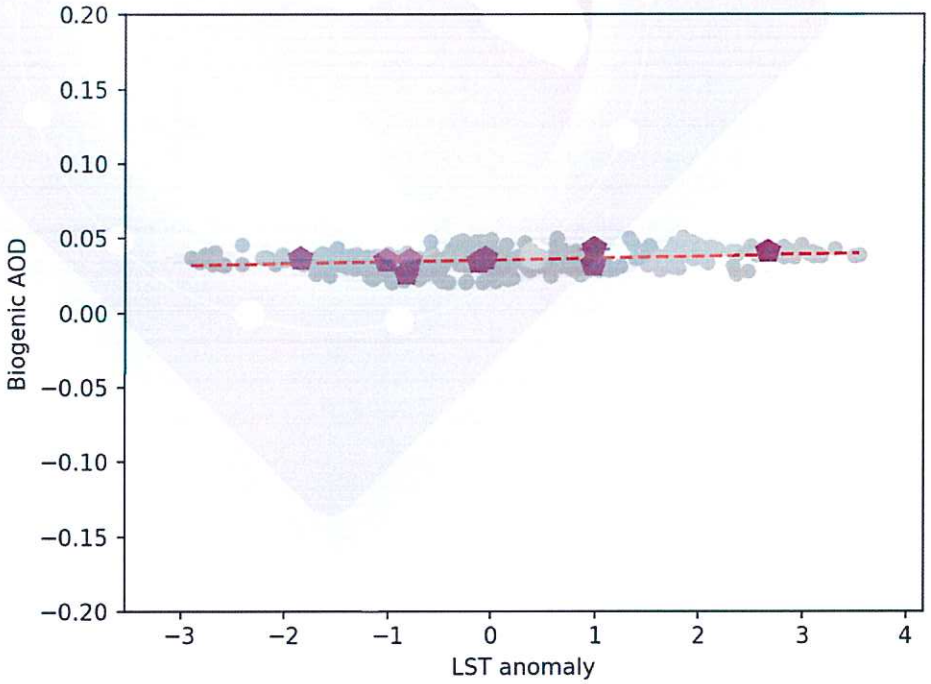

Figure 14. Biogenic AOD (based on the difference between the CONTROL and the noBIOSOA simulations) vs. LST

anomaly for the summers (JJA) of 2002-2010 over eastern Russia. Pentagons represent the averages over the whole domain (78-100°E, 57-63°N) while the dots represent 1.9° × 1.9° pixels within the domain. The dashed line represents the linear fit to the individual pixels ($AOD_{bio} = 0.0012LST_{ano} + 0.035$), the red curtain represents the 90 % credible interval for the linear fit and the error bars represent the uncertainty caused by temporal averaging.

Western Russia

Over the mixed (38 pixels) and evergreen needleleaf (14 pixels) forests in western Russia there are strong positive temperature dependences in summertime AOD as shown in Figures 15 and 16. Over the mixed and evergreen needleleaf forests the AODs increase by (57±6) × 10^{-4} K^{-1} and (47±5) × 10^{-4} K^{-1}, respectively. The AOD values over these land cover types do not exhibit a clear dependence on columnar CO concentrations but over the mixed forests the AOD has a positive dependence on tropospheric NO_2 concentrations: (21±2) × 10^{-17} $(molecules/cm^2)^{-1}$. This indicates that the aerosol population over the mixed forests is most likely influenced by anthropogenic emissions. To remove the anthropogenic contribution from the total AOD we used the same methodology as over the southeastern US. The temperature dependence of the remaining non-anthropogenic AOD over the mixed forests is shown in Figure 17. The slope of this temperature dependence ((67±11) × 10^{-4} K^{-1}) is slightly larger than for the total AOD and in the same range as the slope of non-anthropogenic AOD over the southeastern US. The simulated temperature dependence of the biogenic AOD for the whole region (see Figure 18) is in good agreement with the observations. According to our simulations the biogenic AOD increases (60±7) × 10^{-4} K^{-1}. The slope of the simulated biogenic AOD-LST dependence is between the observed values for the mixed and evergreen needleleaf forests. Due to the coarser resolution of the model we were not able to estimate the simulated AOD-LST relationship for the two forest types separately.

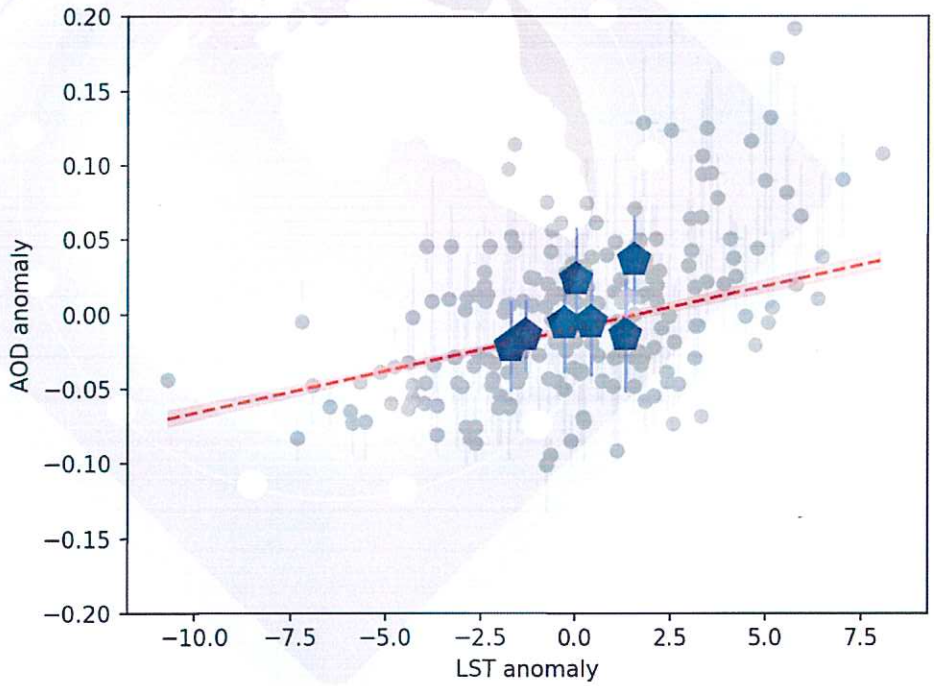

Figure 15. Summertime (JJA) anomalies of total AOD vs. LST, for the years 2005–2011 over mixed forests in western Russia. The AOD and LST are from L3 AATSR. Pentagons represent the averages over the mixed forest pixels (40-65°E, 59-66°N) while the dots represent 1° × 1° pixels within the domain. The dashed line represents the linear fit to the 1° × 1° pixels ($AOD = 0.0057LST_{ano} - 0.009$), the red curtain represents the 90 % credible interval for the linear fit and the error bars represent the uncertainty of the data points.

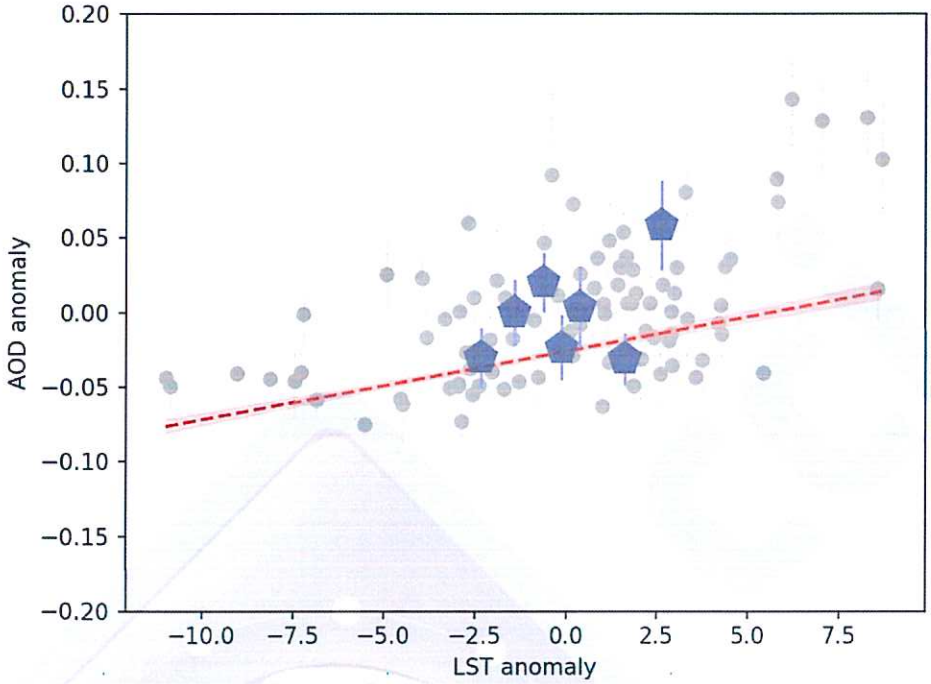

Figure 16. Summertime (JJA) anomalies of total AOD vs. LST, for the years 2005–2011 over evergreen needleleaf forests in western Russia. The AOD and LST are from L3 AATSR. Pentagons represent the averages over the evergreen needleleaf pixels (40-65°E, 59-66°N) while the dots represent 1° × 1° pixels within the domain. The dashed line represents the linear fit to the 1° × 1° pixels ($\mathrm{AOD} = 0.0047\mathrm{LST}_{\mathrm{ano}} - 0.025$), the red curtain represents the 90 % credible interval for the linear fit and the error bars represent the uncertainty of the data points.

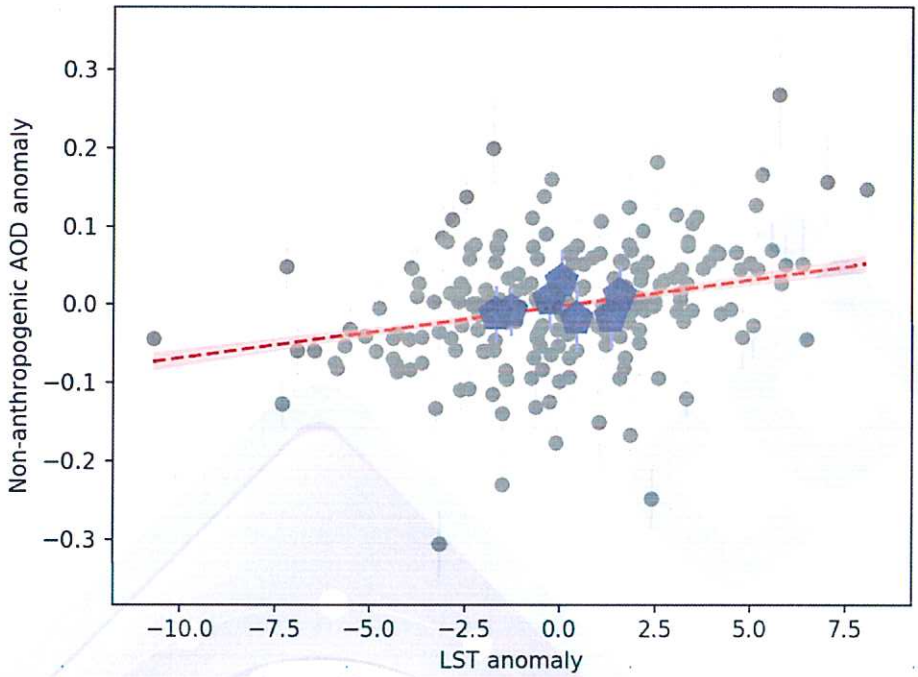

Figure 17. Summertime (JJA) anomalies of non-anthropogenic AOD vs. LST, for the years 2005–2011 over mixed forests in western Russia. The non-anthropogenic AOD is based on L3 AATSR AOD and OMI tropospheric NO_2 observations. LST is from L3 AATSR. Pentagons represent the averages over the mixed forest pixels (40-65°E, 59-66°N) while the dots represent 1° × 1° pixels within the domain. The dashed line represents the linear fit to the 1° × 1° pixels ($AOD_{NA,ano} = 0.0067LST_{ano} - 0.001$), the red curtain represents the 90 % credible interval for the linear fit and the error bars represent the uncertainty of the data points.

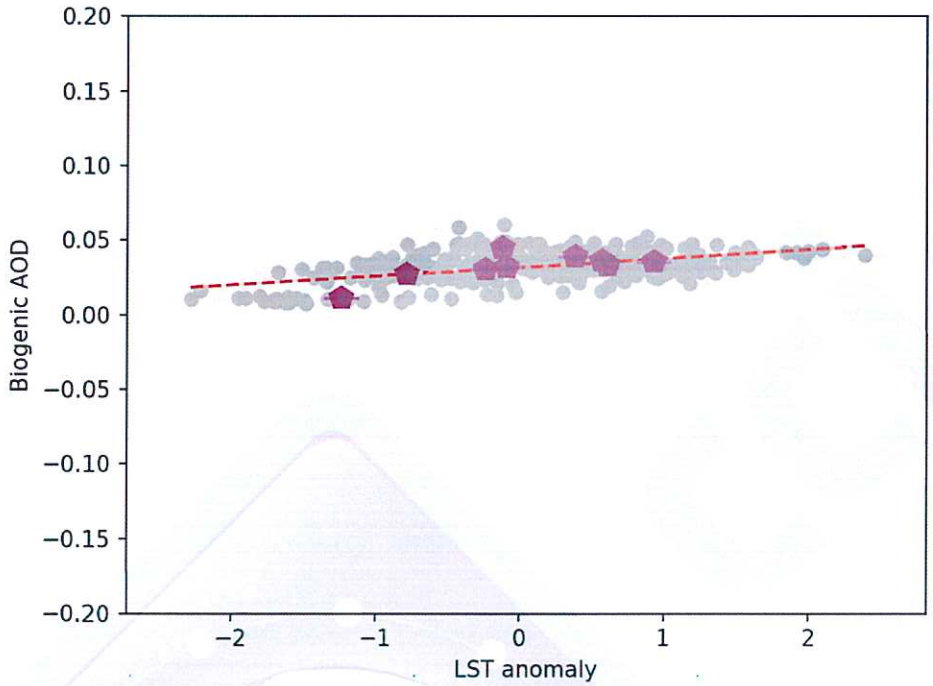

Figure 18. Biogenic AOD (based on the difference between the CONTROL and the noBIOSOA simulations) vs. LST anomaly for the summers (JJA) of 2002-2010 over western Russia. Pentagons represent the averages over the whole domain (40-65°E, 59-66°N) while the dots represent 1.9° × 1.9° pixels within the domain. The dashed line represents the linear fit to the individual pixels ($AOD_{bio} = 0.0060 + 0.032$), the red curtain represents the 90 % credible interval for the linear fit and the error bars represent the uncertainty caused by temporal averaging.

Over these three boreal regions (Canada, Eastern Russia and Western Russia) the model and the observations produce corresponding results although the simulated estimates of the temperature dependence of AOD tend to be slightly smaller. This difference could be caused by limitations in the simulations or in the observations. However, with both methods the same main results are reached:

- the temperature dependence of AOD over the boreal forests is weaker in the regions further away from anthropogenic emissions than in the vicinity of anthropogenic sources,
- the temperature dependence of AOD can be as strong as in the southeastern US.

However, the temperature dependence of the biogenic AOD over the mixed forests in the southeastern US is four to five times stronger than over the boreal forests.

Table 2 presents the radiative effect estimates for the biogenic aerosols based on the observations and simulations. The observational DRE estimates (DRE_{obs}) are calculated with equation 1. Similar to the AOD data sets, the observational and simulated radiative effect estimates are in good agreement and show that the radiative effects are the largest in the vicinity of anthropogenic sources in mixed forests in Western Russia. Our estimates for the DREs are up to 10 times larger than the estimates by Paasonen et al. (2013) and up to 3 times larger than the estimates by Lihavainen et al (2009). Our estimate for Eastern Russia is in reasonable agreement with the estimate for Northern Finland (-0.097±0.066 W/m^2/K) by Lihavainen et al. (2009). Regarding the indirect effects (ERF), the simulations indicate that the effects are positive and larger than the DREs, which implies that direct cooling effects are most likely masked by the warming caused by the indirect effects.

Table 2. Radiative effects of biogenic aerosols three boreal regions and the souteastern US. The region and season averaged incident solar radiation at the top of the atmosphere (S_{rad}) and the mean daytime value of the secant of the solar zenith angle (ϕ) are also shown. The acronyms ENF and MF refer to evergreen needleleaf forest and mixed forest, respectively.

Region	DRE_{obs} [W/m^2/K]	DRE_{sim} [W/m^2/K]	ERF_{sim} [W/m^2/K]	S_{rad} [W/m^2]	ϕ
Canada	-0.05±0.17	-0.138±0.002	0.75±0.07	433	1.64
Eastern Russia	-0.15±0.07	-0.172±0.007	0.18±0.17	427	1.73
Western Russia, ENF	-0.29±0.03	-0.252±0.010	1.30±0.20	422	1.81
Western Russia, MF	-0.41±0.07			422	1.81
Southeastern US	-0.31±0.22	-0.34±0.02	-1.04±0.22	461	1.33

A manuscript describing these results is in preparation.

Work package 3

In the last work package (WP3), we analysed how the temperature dependence of biogenic AOD changes as the global mean temperature increases. Our hypothesis was that in a warmer environment the negative feedback would be larger as the plants emit more VOCs to the atmosphere. Our future simulations showed that the future impacts of biogenic aerosols can be complicated by other mechanisms. To study the difference between the present day and the future, the parameters from the CONTROL simulation were subtracted from the parameters from FUTURE_CONTROL simulation. The biogenic components for the present day and the future were estimated by subtracting the noBIOSOA simulations from the corresponding CONTROL simulations.

The change in average summertime LST is shown in Figure 19. Significant warming is projected for most regions but there is cooling in the southeastern US and to a smaller extent in the boreal regions in Russia. Thus, although the climate warms as a whole, there are significant regional differences which reflect the natural emissions. Overall, plants emit more VOCs in a warmer climate as can be seen in Figure 20. However, the increase in VOCs does not translate to such a large increase in the biogenic aerosol burden and according to these simulations, the burden can decrease over some regions (e.g. the southeastern US) when compared to the present day (Figure 21). The decrease in the biogenic aerosol burden over the southeastern US is most likely caused by the decrease in LST in this region (see Figure 19). However, the cooling of this region in the future is highly uncertain and it could be caused by the projected sea surface temperature used as an input in these simulations.

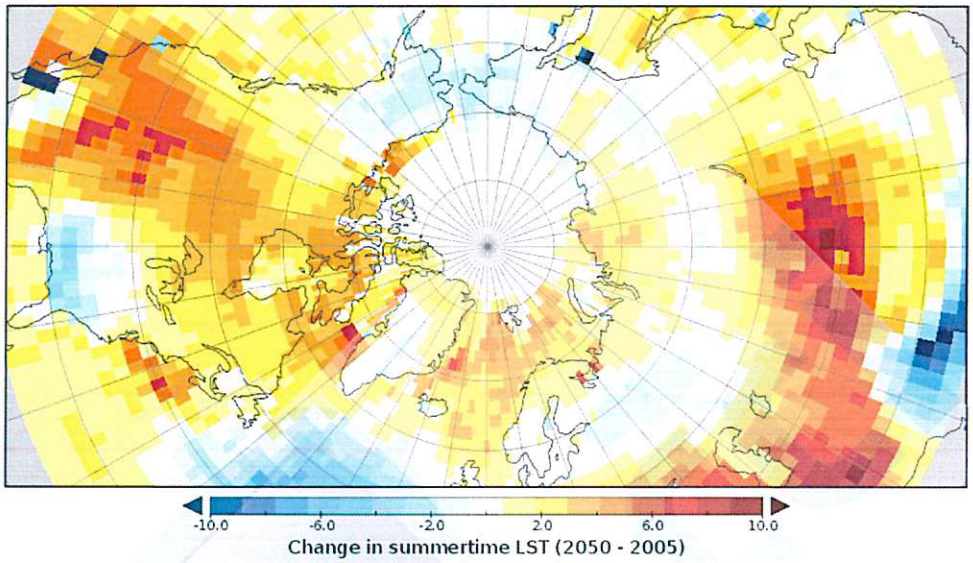

Figure 19. Difference in the future and the present day summertime (JJA) averaged land surface temperature. For the year 2050 the RCP8.5 scenario is used.

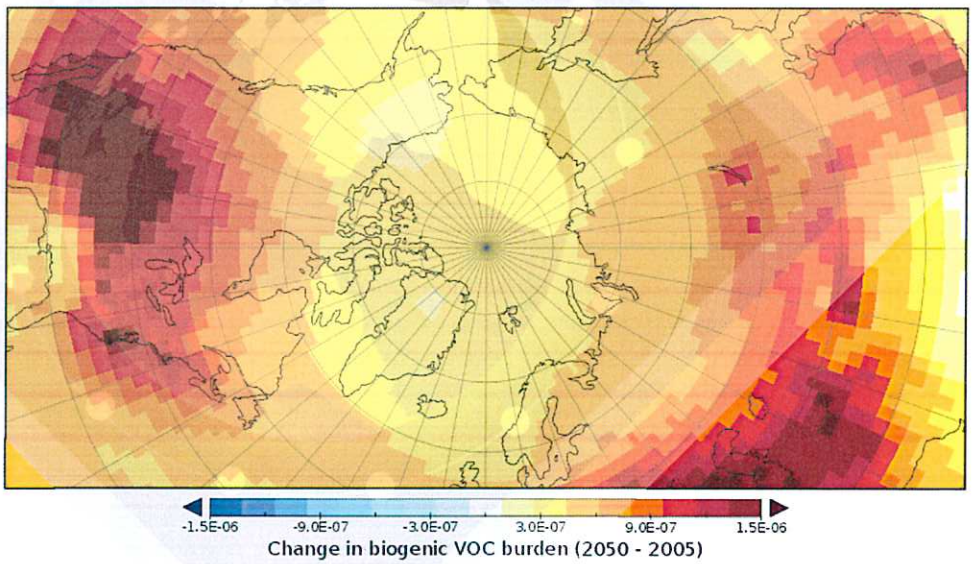

Figure 20. Difference in the future and the present day summertime (JJA) averaged biogenic VOC burden. For the year 2050 the RCP8.5 scenario is used.

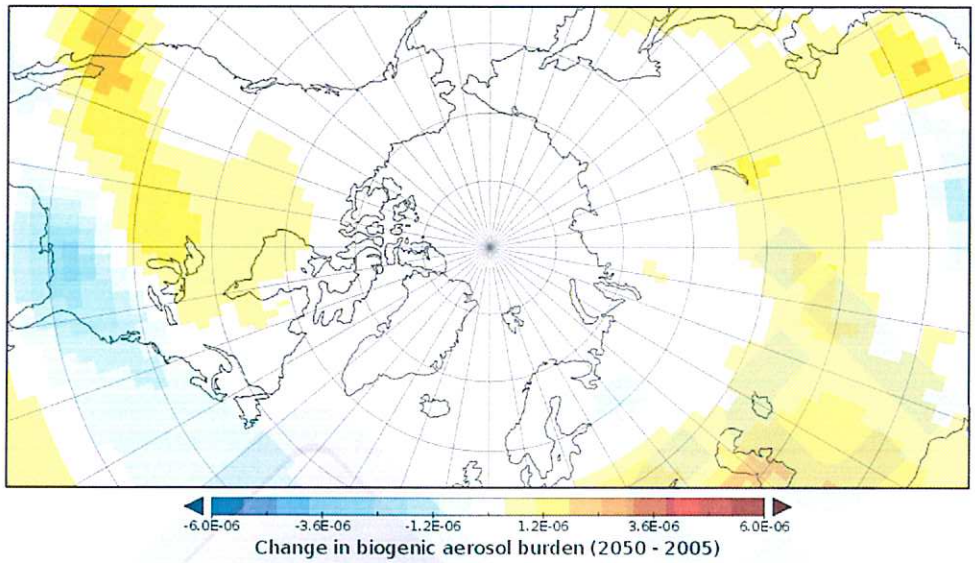

Figure 21. Difference in the future and the present day summertime (JJA) averaged burden of biogenic aerosols. For the year 2050 the RCP8.5 scenario is used.

The comparison of the future and the present day biogenic AODs is shown in Figure 22. As the figure shows, the biogenic AOD over the northern latitudes decreases. The reduction the in biogenic AOD is clearer than in the biogenic aerosol burden (Figure 21) which is most likely caused by changes is the aerosol size distributions. Considering the same amount of VOCs on smaller particles can affect the AOD less than VOCs condensed on larger particles. The two major causes for this unexpected decrease in biogenic AOD are gas-to-particle partitioning and the total aerosol load. In a warmer climate the VOCs do not condense on existing particles as easily as their saturation vapour pressure increases and in thermodynamical equilibrium a much larger fraction of the VOCs remain in the gas phase (Hennigan et al., 2009). Secondly, the anthropogenic aerosol emissions are expected to be lower in the future which means that there are less aerosols for the VOCs to condense on. Consequently, the biogenic AOD decreases in the future.

Although most future studies indicate that the biogenic aerosols would introduce a stronger negative feedback in the future (e.g. Jiang et al., 2010; Heald et al., 2008; Tsigaridis and Kanakidou, 2007), Lin et al. (2016) reached a conclusion similar to that from this work. They used the Community Earth System Model (CESM) and found that the global SOA burden is most sensitive to climate change (meaning temperature and CO_2 concentration), followed by anthropogenic land use and land cover change. On a global scale, there is only a small increase in the SOA burden: in South Asia and Tropical Pacific Ocean the SOA burden increases but in the US, Europe and East Asia it decreases. Our biogenic AOD estimates lead to the same conclusions although the mechanism which we consider is different. Furthermore, we calculated the temperature dependence of biogenic AOD for the regions we had analysed in WP1 and WP2. The biogenic AOD exhibited a temperature dependence over western Russia ($(38\pm7) \times 10^{-4}$ K^{-1}), eastern Russia ($(11\pm5) \times 10^{-4}$ K^{-1}) and Canada ($(9\pm1) \times 10^{-4}$ K^{-1}) but the dependencies were smaller than the corresponding dependencies simulated for the present day. The decrease in the slope was larger over western Russia because there the anthropogenic emissions had a larger contribution in the temperature dependence of AOD and the emissions were lower in the future scenario. Over the southeastern US biogenic AOD did not exhibit any temperature dependence.

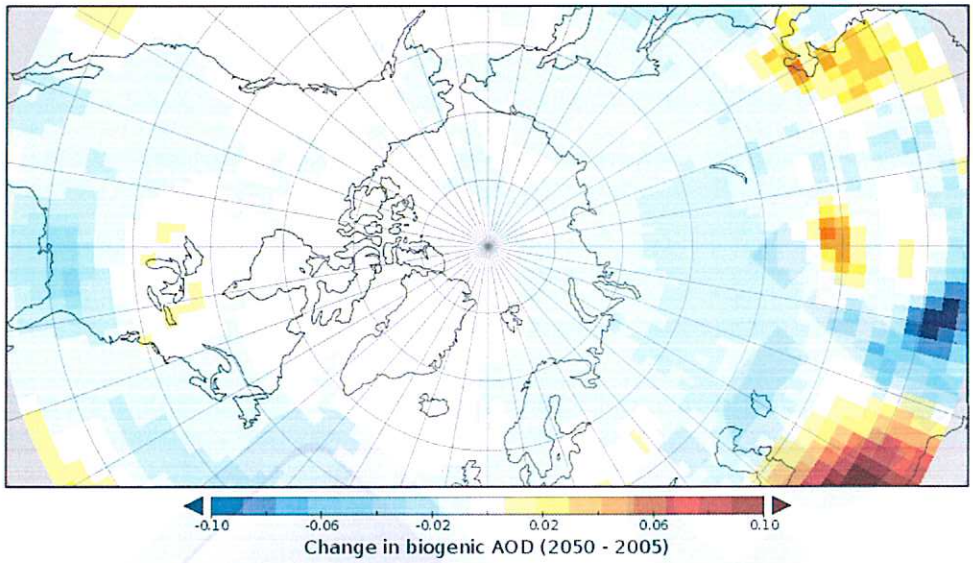

Figure 22. Difference in the future and the present day summertime (JJA) averaged biogenic AOD. For the year 2050 the RCP8.5 scenario is used.

In addition to the direct radiative effects, the negative feedback of the biogenic aerosols could come from their effect on clouds. Therefore, we estimated how the biogenic contribution to the burden of cloud droplet number concentration (CDNC) could change in the future. This comparison is shown in Figure 23. The biogenic CDNC burden decreases even more systematically than the biogenic AOD. This indicates that the biogenic emissions will not be able to slow down climate change in the future.

A manuscript describing these results is in preparation.

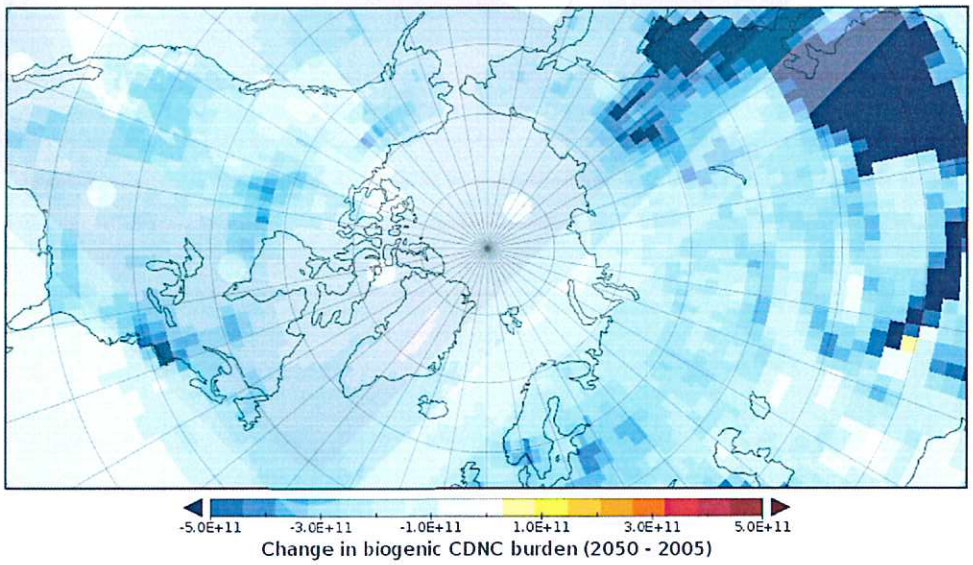

Figure 23. Difference in the future and the present day summertime (JJA) averaged biogenic CDNC burden. For the year 2050 the RCP8.5 scenario is used.

Conclusions

In the ITICA project we have studied the temperature dependence of AOD in the southeastern US and over boreal regions using spaceborne observations and climate model simulations. The observations and simulations produced corresponding results in all studied regions. The main conclusions of this study are:

- AOD exhibited temperature dependent behaviour which is most likely caused by biogenic emissions.
- The temperature dependence of biogenic AOD is stronger in the presence of anthropogenic aerosols
- The temperature dependent biogenic AOD has significant radiative effects in the present day climate but the significance decreases in the future, thus biogenic aerosols do not appear to produce a strong negative climate feedback. This contradicts with the hypothesis that increased biogenic emissions in the future could slow down global warming.

Contribution and cooperation with CCI Project Teams and potential feedback of research

Regarding the usage of AATSR AOD data, the fellow has worked in close collaboration with members of the Aerosol_cci team (Dr. Kolmonen, Dr. Sogacheva). For example, during the project we have evaluated the different AATSR retrievals using AOD data from MISR. There has not been real collaboration with the SM_cci team because the soil moisture data did not provide significant information for the study over SEUS. Dr. Darren Ghent from the GlobTemperature project has been a valuable collaborator regarding the usage of the AATSR LST data.

References

Aaltonen, V., E. Rodriguez, S. Kazadzis, A. Arola, V. Amiridis, H. Lihavainen, and G. de Leeuw (2011). On the variation of aerosol properties over Finland based on the optical columnar measurements. Atm. Res., 116, 46-55.

Albrecht, B.A. (1989). Aerosols, Cloud Microphysics, and Fractional Cloudiness. Science 245 (4923): 1227–30.

Bergman T., Kerminen V.-M., Korhonen H., Lehtinen K. E. J., Makkonen R., Arola A., Mielonen T., Romakkaniemi S., Kulmala M., Kokkola H. (2012) Evaluation of the sectional aerosol microphysics module SALSA implementation in ECHAM5-HAM aerosol-climate model. Geosci. Model. Dev., 5, 845 – 868; doi:10.5194/gmd-5-845-2012.

Carslaw, K. S, Lee, L. A., Reddington, C. L., Pringle, K. J., Rap, A., Forster, P. M., Mann, G. W., Spracklen, D. V., Woodhouse, M. T., Regayre, L. A., Pierce, J. R. (2013). Large contribution of natural aerosols to uncertainty in indirect forcing. Nature, 503, 67-71.

Charlson et al., (1992). Charlson, R. J., Schwartz, S. E., Hales, J. M., et al. (1992). Climate forcing by anthropogenic aerosols. Science 255, 423–430.

de Gouw et al. (2005), Budget of organic carbon in a polluted atmosphere: Results from the New England Air Quality Study in 2002, J. Geophys. Res., 110, D16305, doi:10.1029/2004JD005623.

Donahue, N. M., Epstein, S. A., Pandis, S. N., and Robinson, A. L. (2011). A two-dimensional volatility basis set: 1. organic-aerosol mixing thermodynamics, Atmos. Chem. Phys., 11, 3303-3318.

Duncan, B. N., Y. Yoshida, M. R. Damon, A. R. Douglass, and J. C. Witte (2009). Temperature dependence of factors controlling isoprene emissions, Geophys. Res. Lett., 36, L05813.

Emde, C., Buras-Schnell, R., Kylling, A., Mayer, B., Gasteiger, J., Hamann, U., Kylling, J., Richter, B., Pause, C., Dowling, T., and Bugliaro, L. (2016). The libRadtran software package for radiative transfer calculations (version 2.0.1), Geosci. Model Dev., 9, 1647-1672, doi:10.5194/gmd-9-1647-2016.

Ford, B. and Heald, C. L., 2013, Aerosol loading in the Southeastern United States: reconciling surface and satellite observations, Atmos. Chem. Phys., 13, 9269-9283.

Ghent, D. Land Surface Temperature Validation and Algorithm Verification (Report to European Space Agency), 2012.

Goldstein, A.H., C.D. Koven, C.L. Heald, I. Fung (2009). Biogenic Carbon and Anthropogenic Pollutants Combine to Form a Cooling Haze over the Southeastern US, Proceedings of the National Academy of Sciences, 106, 8835-8840.

Guenther, A., Karl, T., Harley, P., Wiedinmyer, C., Palmer, P. I., and Geron, C. (2006). Estimates of global terrestrial isoprene emissions using MEGAN (Model of Emissions of Gases and Aerosols from Nature), Atmos. Chem. Phys., 6, 3181-3210, doi:10.5194/acp-6-3181-2006.

Haywood, J. M., and Shine, K. P. (1995). The effect of anthropogenic sulfate and soot aerosol on the clear sky planetary radiation budget, Geophys. Res. Lett., 22, 603–606.

Heald, C. L., et al. (2008). Predicted change in global secondary organic aerosol concentrations in response to future climate, emissions, and land use change, J. Geophys. Res., 113, D05211, doi:10.1029/2007JD009092.

Hennigan, C. J., Bergin, M. H., Russell, A. G., Nenes, A., and Weber, R. J. (2009). Gas/particle partitioning of water-soluble organic aerosol in Atlanta, Atmos. Chem. Phys., 9, 3613-3628, doi:10.5194/acp-9-3613-2009.

International Panel on Climate Change (2013). Climate Change 2013: The Physical Science Basis. Contribution of Working Group I to the Fifth Assessment Report of the Intergovernmental Panel on Climate Change, edited by: Stocker, T. F., Qin, D., Plattner, G.-K., Tignor, M., Allen, S. K., Boschung, J., Nauels, A., Xia, Y., Bex, V., and Midgley, P. M., Cambridge University Press, Cambridge, United Kingdom and New York, NY, USA, 1535 pp.

Jiang, X., Yang, Z.-L., Liao, H., Wiedinmyer, C. (2010). Sensitivity of biogenic secondary organic aerosols to future climate change at regional scales: An online coupled simulation, Atmos. Environ., 44, 38, 4891-4907, https://doi.org/10.1016/j.atmosenv.2010.08.032.

Kolmonen, P., L. Sogacheva, T.H. Virtanen, G. de Leeuw and M. Kulmala (2016). The ADV/ASV AATSR aerosol retrieval algorithm: current status and presentation of a full-mission AOD data set. International Journal of Digital Earth, 9:6, 545-561,DOI: 10.1080/17538947.2015.1111450.

Laakso, A., Kokkola, H., Partanen, A.-I., Niemeier, U., Timmreck, C., Lehtinen, K. E. J., Hakkarainen, H., and Korhonen, H. (2016). Radiative and climate impacts of a large volcanic eruption during stratospheric sulfur geoengineering, Atmos. Chem. Phys., 16, 305-323, doi:10.5194/acp-16-305-2016.

Leaitch, W. R. et al., (2011). Temperature response of the submicron organic aerosol from temperate forests, Atmos Env., 45, 6696-6704.

Lihavainen, H., Asmi, E., Aaltonen, V., Makkonen, U. and Kerminen, V.-M. (2015). Direct radiative feedback due to biogenic secondary organic aerosol estimated from boreal forest site observations, Environ. Res. Lett. 10, 104005.

Lin, G., J. E. Penner, and C. Zhou (2016). How will SOA change in the future?, Geophys. Res. Lett., 43, 1718–1726, doi:10.1002/2015GL067137.

Millet, D., Jacob, D., Boersma, F., Fu, T.-M., Kurosu, T., Chance, K., Heald, C., and Guenther, A. (2008). Spatial distribution of isoprene emissions from North America derived from formaldehyde column measurements by the OMI satellite sensor, J. Geophys. Res., 113, D02307, doi:10.1029/2007JD008950

Paasonen, P., Asmi, A., Petäjä, T., Kajos, M. K., Aijala, M., Junninen, H., Holst, T., Abbatt, J. P. D., Arneth, A., Birmili, W., van der Gon, H. D., Hamed, A., Hoffer, A., Laakso, L., Laaksonen, A., Leaitch, W. R., Plass-Duelmer, C., Pryor, S. C., Raisanen, P., Swietlicki, E., Wiedensohler, A., Worsnop, D. R., Kerminen, V.-M., and Kulmala, M. (2013). Warming-induced increase in aerosol number concentration likely to moderate climate change, Nature Geoscience. 6, 6, 438-442.

Penuelas, J. and Staudt, M., 2010, BVOCs and global change, Trends in Plant Sci., 15, 133-144.

Prata, F. Land Surface Temperature Measurement from Space: AATSR Algorithm Theoretical Basis Document, 2002.

Slowik, et al., 2010, Characterization of a large biogenic secondary organic aerosol event from eastern Canadian forests, Atmos. Chem. Phys, 10, 2825-2845.

Spracklen, D.V., Bonn, B., and Carslaw, K.S. (2008) Boreal forests, aerosols and the impacts on clouds and climate, Phil. Trans. R. Soc. A., 366, 4613-4626.

Stevens, B., and G. Feingold (2009). Untangling aerosol effects on clouds and precipitation in a buffered system. Nature, 461, doi:10.1038/nature08281

Stier, P., Feichter, J., Kinne, S., Kloster, S., Vignati, E., Wilson, J., Ganzeveld, L., Tegen, I., Werner, M., Balkanski, Y., Schulz, M., Boucher, O., Minikin, A., Petzold, A. (2005) The aerosol-climate model ECHAM5-HAM. Atmos. Chem. Phys., 5, 1125–1156; doi:10.5194/acp-5-1125-2005.

Stroud et al. (2007). Cloud Activating Properties of Aerosol Observed during CELTIC, Journal of Atmospheric Sciences, 64, 441-459, 10.1175/JAS3843.1

Tsigaridis, K., and Kanakidou, M. (2007). Secondary organic aerosol importance in the future atmosphere, Atmos. Environ., 41, 22, 4682-4692, https://doi.org/10.1016/j.atmosenv.2007.03.045.

Tunved, P., Hansson, H. C., Kerminen, V-M., Strom, J., Dal Maso, M., Lihavainen, H., Viisanen, Y., Aalto, P. P., and Komppula, M., Kulmala, M. (2006). High natural aerosol loading over boreal forests. Science, 312(5771), 261-263. 10.1126/science.1123052.

Twomey, S. (1991). Aerosols, clouds, and radiation. Atmos. Environ., 25, 2435–2442.

Veefkind, J. P., Boersma, K. F., Wang, J., Kurosu, T. P., Krotkov, N., Chance, K., and Levelt, P. F. (2011) Global satellite analysis of the relation between aerosols and short-lived trace gases, Atmos. Chem. Phys., 11, 1255-1267, doi:10.5194/acp-11-1255-2011.

Zhang, K., O'Donnell, D., Kazil, J., Stier, P., Kinne, S., Lohmann, U., Ferrachat, S., Croft, B., Quaas, J., Wan, H., Rast, S., and Feichter, J. (2012) The global aerosol-climate model ECHAM-HAM, version 2: sensitivity to improvements in process representations. Atmos. Chem. Phys, 12, 8911–8949; doi:10.5194/acp-12-8911-2012.

Zhang, Q., Parworth, C., Lechner, M. and Jimenez, J.L. (2017). Aerosol Mass Spectrometer Global Database. https://sites.google.com/site/amsglobaldatabase